Post-print of: Biernat J., Nazaruk E.: Voltammetric and biological studies of folate-targeted non-lamellar lipid mesophases ELECTROCHIMICA ACTA Vol. 299 (2019), pp.1-11 DOI: https://doi.org/10.1016/j.electacta.2018.12.164

Voltammetric and biological studies of folate-targeted non-lamellar lipid mesophases

Marlena Godlewska [a], Agnieszka Majkowska-Pilip [b], Anna Stachurska [c], Jan F. Biernat [d], Damian Gaweł [a, **], Ewa Nazaruk [e, *]

[a] Department of Biochemistry and Molecular Biology, Centre of Postgraduate Medical Education, Marymoncka 99/103, 01-813, Warsaw, Poland [b] Centre of Radiochemistry and Nuclear Chemistry, Institute of Nuclear Chemistry and Technology, Dorodna 16, 03-195, Warsaw, Poland [c] Department of Immunohematology, Centre of Postgraduate Medical Education, Marymoncka 99/103, 01-813, Warsaw, Poland [d] Chemical Faculty, Gdansk University of Technology, Narutowicza 11/12, Gdansk, 80-233, Poland [e] Faculty of Chemistry, University of Warsaw, Pasteura 1, 02-093, Warsaw, Poland

Abstract:

Folate-targeted lipid nanostructures are promising strategies for the development of biocompatible drug delivery systems. The objective of this study was to evaluate the efficacy of drug delivery to cancer cells by folate-targeted lipid mesophases, cubosomes (CUB) and hexosomes (HEX), loaded with doxorubicin (DOX). Three cancer-derived cell lines (KB, HeLa, T98G) exhibiting different expressional levels of folate receptor protein (FR) were used. DOX-loaded folate-targeted CUB and HEX dispersions were characterized via small angle X-ray scattering and dynamic light scattering to assess their physicochemical properties. DOX release characteristics were evaluated by electrochemical methods and demonstrated structure-dependent release capabilities. A slow release rate was observed for hexosomes, while cubosomes offered more rapid drug transport. Analysis of the release kinetics revealed that the total amount of DOX released from cubosomes is linearly dependent on the square root of time, implying that the release process follows the Higuchi diffusion model. Assessment of drug uptake performed on cancerderived cell lines demonstrated that DOX accumulation in cancer cell depends not only on the release capability of the applied mesophase, but also, on the level of folate receptor protein present in the cancer cells. FR-functionalized CUB and HEX enabled faster drug delivery to cancer cells as a result of receptorligand interactions. In addition, doxorubicin encapsulated into FR-cubosomes demonstrated significantly improved anti-tumor activity promoting the necrosis of tumor cells, while DOX-loaded FA-hexosomes acted via induction of the apoptotic state. Overall, our data indicates that folate-modified formulations are promising drug delivery systems and can be considered as potential therapeutic tools in the targeted therapy of FR-positive tumors.

Keywords: Cubosome, Hexosome, Drug delivery, Doxorubicin, Folate-targeted lipid nanostructures

1. Introduction

The growing interest in lipidic cubic and hexagonal mesophases observed over the last decade is associated with their promising applications in medicine. Such systems display structures similar to those observed in biological membranes and their ordered organization allows for protection of the carried biological compounds [1,2]. They present a high drug delivery potential as they can be accumulated in cancer cells due to enhanced permeability and retention effect (EPR). Therefore, the chemotherapeutic can be accumulated at a desired site and released on demand via an external stimulus. The greater selectivity of drug delivery may be achieved by design of targeted materials able to increase the affinity for specific tumor cells. Utilization of lipid non-lamellar liquid crystalline nanostructures (LLC NPs) as drug delivery systems (DDS) offers advantages of high cargo loading capacity and controlled release through appropriate functionalization [2e4].

Lipids, when placed in water, can adopt different structural organizations, the most common ones being the inverted cubic (V2) and inverted hexagonal (H2) phase [1]. The H2 phase consists of closed reverse micellar cylinders that are arranged in a 2D hexagonal lattice. 3D-ordered structures include micellar cubic (I2) and bicontinuous cubic phase (V2) structures (including the primitive (P, Im3m), diamond (D, Pn3m) and gyroid (G, Ia3d) cubic phases) [1]. The inverted bicontinuous V2 mesophase consists of two interpenetrating, but unconnected, aqueous channels surrounded by a lipid bilayer. Such compartmentalization in lipid mesophases can be used to introduce cargos of hydrophilic, lipophilic or amphiphilic properties. The release rate of drug from liquid crystalline systems can be manipulated by changing variables such as temperature, pressure, pH or their composition [5e9]. Therefore, drug release from the bicontinuous cubic phase may be significantly faster than from the other mesophases [10,11]. In addition, the structural parameters of mesophases can be adjusted and targeted towards the specific requirements of the drug release by changing their curvature to affect the bilayer thickness, water channel diameter, and unit cell size. These factors can be predicted based on Israelachvili's concept [12] known as the critical packing parameter (CPP ¼ v/a l, where v is the effective volume, a is the head-group area and l is the chain length). Amphiphiles with the smaller hydrophilic heads (CPP[1) should lead to the formation of highly negatively curved hexagonal (H2) or micellar cubic mesophases (I2). Formation of more swollen cubic systems can be obtained by additives with CPP<1, which promote the fine flattering of the membrane's curvature [13,14].

Overall, nanoparticles, which actively target tumor cells and increase the efficiency of cancer treatment, can be obtained by conjugation of the nanoparticles with ligands that bind to specific receptors overexpressed on the tumor cells. Cubosomes (CUB) and hexosomes (HEX), nanoparticles containing the inverse cubic phase or the inverse hexagonal phase, respectively, are promising strategies for the development of such targeted lipid-based DDS, as they can be functionalized with e.g. biotin or folic acid (FA) and used for imaging and active targeting of the receptors overexpressed by cancer cells [15e20]. Also, paclitaxel (PX)-loaded cubosomes, functionalized with an antibody presented high affinity for an epidermal growth factor receptor (EGFR) and showed significantly higher cytotoxicity than a free drug formulation against ovarian cancer cells [16]. Moreover, PX-loaded biotinylated cubosomes presented decreased drug toxicity due to enhanced efficacy of PX against tumor cells. This was caused by the biotin ligand-promoted drug uptake by cancer cells via receptor-mediated endocytosis [17]. Other recent studies on the preparation of folatemodified cubosomes or hexosomes showed that the folatemodified cubosomes containing etoposide or camptothecin present faster uptake as a result of receptor-ligand interactions [18e20].

In our previous studies, we investigated application of lipidic cubic phases for controlled delivery of doxorubicin (DOX) - an anticancer drug [21e23]. We used electrochemical methods to determine diffusional properties of DOX and other compounds in different cubic mesophases. More recently, we showed that hexosomes are promising DOX-delivery vehicles, characterized by a prolonged release capability [24]. In this work, we extended our previous studies and performed a more

detailed analysis, applying a range of in vitro assays to evaluate the effect of folatefunctionalized cubosomes and hexosomes on the DOX uptake and viability of tumor cells. The structure of the folate-conjugated nanoparticles was verified by means of small angle X-ray scattering, while electrochemical techniques were used to determine the kinetics and drug release properties. The biological studies were carried out on three cancer-derived cell lines exhibiting different expressional levels of folate receptor protein (FR). We found that efficiency of DOX uptake depends not only on the release capability of the applied mesophase, but also on the level of folate receptor protein present in the cells. Moreover, it was demonstrated that exposure of the cells to an excess concentration of folic acid effectively saturated the cell's FR, resulting in the inhibition of the binding properties of folate-modified phases. Finally, we established that DOX-loaded folate-modified hexosomes induce the apoptotic state in tumor cells via prolonged drug release. The obtained data indicates that FA-mediated acquisition of drug encapsulated in the lipid mesophases can be considered as a potential strategy for targeted delivery of chemotherapeutics to FRpositive cells.

2. Experimental section

2.1. Materials

Monoolein (1-oleoyl-rac-glycerol) purity 99% (GMO), tetradecane (TD), 2-(N-morpholino) ethanesulfonic acid (MES), doxorubicin hydrochloride (DOX) and Pluronic F108 (PF108), used for the synthesis of the mesophases, were purchased from SigmaAldrich (USA). Schemes of the compounds used are shown in S1. All solutions were prepared with Milli-Q water (18.2 MU cm^{1}; Millipore, USA).

2.2. Preparation of nanostructures (NPs)

To produce folate-functionalized LLC nanoparticles, folic acid was conjugated with a stabilizer, Pluronic F108. Thus, folic acid attached to the LLC nanoparticles was exposed to the solution and had a favorable orientation for recognition by the FR. Folatefunctionalized Pluronic F108 (PF108-FA) was synthesized according to the procedure described by Caltagirone and co-workers [18]. The chosen ratio of the stabilizer mixture PF108/PF108-FA was 4/1. This ratio was selected due to the observation that in case of low ligand densities, contribution of active vs. passive targeting seems to be higher than in case of higher ligand densities [25].

2.2.1. Preparation of cubosomes

A method utilizing the top-down approach was used to obtain cubosomes. They were produced by hydrating the lipid in the presence of stabilizer Pluronic F108 or mixture of Pluronic F108 with folate-functionalized Pluronic F108-FA (PF108/PF108-FA). Then, the hydrated lipid was sonicated using SONICS Vibracell VCX 130 (Sonics & Materials Inc., USA). To prepare DOX-loaded cubosomes (CUB/DOX and CUB/DOX/FA), doxorubicin was mixed with melted lipid before hydration.

2.2.2. Preparation of hexosomes

Hexosomes were prepared similarly to cubosomes, but instead of pure GMO, a mixture of GMO and tetradecane was used. The GMO/TD mixture was prepared by heating the GMO and TD at 54 C (GMO/TD ratio 3/1 w/w). The sample was then vortexed and a polymer solution was added. The emulsification was conducted using SONICS Vibracell VCX 130 (Sonics & Materials Inc.). To prepare DOX-loaded hexosomes (HEX/DOX and HEX/DOX/FA), doxorubicin was mixed with the melted lipid before hydration.

All dispersions were prepared with a lipid content of 5 wt %. The lipid to DOX ratio was maintained at a constant level throughout the entire experiment.

2.3. Characterization of the mesophase systems

Small angle X-ray scattering (SAXS) was applied to verify the structure of folate-functionalized nanoparticles [24,26]. SAXS diffraction patterns were recorded using a Bruker Nanostar system working with CuKa radiation, equipped with a Vantec 2000 area detector. The 2D pattern was integrated into a 1D scattering function I(q), (where q (nm^{1}) is the length of the scattering vector). The scattering vector, q, was determined from the scattering angle using the relationship q¼(4p/l)sinq, with 2q being the scattering angle and l being the wavelength of radiation. The samples were loaded into 1.5 mm capillaries before measurement and left to equilibrate at room temperature for at least 12 h. Measurements were performed at 25 C and the scattered intensity was collected over 2 h.

The DOX entrapment efficiency (EE [%]) of the prepared cubosomes and hexosomes was determined, as described previously [24]. Cubosomes/hexosomes with incorporated DOX were separated from excess of DOX using ultra-centrifugation method. Briefly, cubosome/hexosome dispersions were placed in Amicon tubes (Amicon® Ultra 0.5 mL Centrifugal Filters) and centrifuged at 5000 rpm to separate unbound drug. The supernatant solution was then separated and the amount of free DOX was determined using a UV/Vis spectrophotometer (Cary 60, Agilent) at l¼ 490 nm. The total amount of drug was determined after addition of methanol to cubosomal/hexosomal dispersions (methanol was used to disrupt the nanoparticles). Finally, the amount of DOX loaded into cubosome/hexosome dispersions was calculated by subtracting the amount of free drug from the total amount of drug and divided by the total amount of drug.

The hydrodynamic particle size and polydispersity (PDI) of nanoparticles were assessed through the dynamic light scattering (DLS; Zetasizer Nano ZS Malvern, UK) at 25 C, assuming a viscosity of pure water. The results were presented as an average of three separate experiments.

2.4. Electrochemistry

Electrochemical measurements were recorded using a CHI bipotentiostat with a standard three-electrode arrangement. The working electrode was a glassy carbon electrode (GCE). A silver/ silver chloride electrode (Ag/AgCl) was used as the reference, while a platinum foil was chosen as the counter electrode. Before the experiments, the working electrode was polished on a polishing cloth composed of decreasing alumina particle size (from 0.3 to 0.05 mm). The electrodes were subsequently sonicated to remove the adhered alumina particles, rinsed with ethanol and water, and left to dry. To obtain the release profile from the dispersed

systems, nanoparticles with DOX were placed in the dialysis membrane (MWCO 12e14 kDa) and submerged in 50 ml of MES buffer, pH 5.6. The dialysis membrane was used to prevent adsorption of the drug and lipid on the electrode surface. To determine the release rate of DOX from the DOX-loaded nanoparticles, square wave voltammetry (SWV) was applied. Prior to measurements, the supporting electrolyte was deoxygenated by purging with argon (99.999%) for 15 min. The argon was then passed over the solution surface. For each type of measurements, triplicate experiments were performed.

2.5. Cell lines and culture conditions

HeLa (cervical carcinoma) and T98G (glioblastoma) cell lines were purchased from ATCC (American Type Culture Collection; USA), while KB (cervical carcinoma cell line) cells were obtained from DSMZ (Leibniz Institute DSMZ-German Collection of Microorganisms and Cell Cultures; Germany). T98G and KB cells were cultured in EMEM (Eagle's Minimum Essential Medium; ATCC), whereas HeLa cells were grown in RPMI 1640 medium (Biological Industries, Israel). Growth media were additionally supplemented with 10% (v/v) fetal bovine serum (FBS; Biological Industries) and 100 mg/mL antibiotics (penicillin and streptomycin; Biological Industries). All cells were grown in a humidified incubator at 37 C with 5% CO_2 atmosphere.

2.6. Western blot analysis

For the detection of the folate receptor protein, all cell lines were seeded (5.0 10^5 cells/well) in 6-well plates in RPMI 1640 medium without folic acid (w/o FA) (ThermoScientific, USA) supplemented with 10% FBS (Biological Industries) and 100 mg/mL antibiotics (Biological Industries). After 24 h, cells were lysed and the concentration of proteins was determined as previously described [27]. Proteins (20 mg) were separated by SDS-PAGE (10%) under reducing conditions and blotted onto nitrocellulose membranes. After 1h blocking in 5% (w/v) non-fat milk in Tris-buffered saline (TBS) with 0.1% (v/v) Tween 20 (TBS-T 0.1%), the membranes were probed with primary antibodies: rabbit polyclonal antibody to folate binding protein (0.25 mg/mL; #ab67422; Abcam, UK) or mouse monoclonal anti-b-actin (0.5 mg/mL; #ab6276; Abcam) in blocking buffer overnight at 4 C. Then, the membranes were incubated for 1 h with HRP-conjugated goat anti-rabbit IgG (Dako, Denmark) or HRPconjugated rabbit anti-mouse IgG (JacksonImmuno Research, USA) diluted 1:10000 in the blocking buffer, respectively. The signals were then developed using SuperSignal West Pico Chemiluminescent Substrate (ThermoScientific).

2.7. Doxorubicin intracellular intake assay

The study of accumulation of DOX in cells was performed using a fluorescence assay. 2.5 10^4 cells were seeded in each well of a 96-well plate in complete RPMI 1640 medium w/o FA and cultured for 24 h. Next, the medium was replaced with 100 mL of fresh medium supplemented with drug-loaded nanoparticles (7.2 mL/mL; DOX concentration - 1.4 mM). Following incubation for 2 h, the cells were washed twice with phosphate-buffered saline (PBS) followed by 10-min treatment with 5% SDS (w/v; Sigma-Aldrich). The doxorubicin fluorescence emission was measured at 570 nm in the Synergy H4 multimode microplate reader (Biotek, USA).

2.8. Confocal microscopy

The intracellular accumulation rate of DOX was monitored using confocal microscopy, as already described [24]. Briefly, 24 h before the experiment, 2.0 10^5 cells (per well) were seeded in complete RPMI 1640 medium w/o FA on uncoated cover glasses placed in a 6well plate. After 20 h of incubation, the cells were treated with empty nanoparticles (7.2 mL/mL) or drug-loaded nanoparticles (7.2 mL/mL; DOX concentration - 1.4 mM). In blocking experiments, cells were seeded in RPMI 1640 medium supplemented with 10% FBS (Biological Industries) and 100 mg/mL antibiotics (Biological Industries) and subsequently treated with CUB/DOX/FA or HEX/ DOX/FA. Cover glasses were harvested after 2-h incubation, washed with PBS and fixed with 4% (w/v) paraformaldehyde (SigmaAldrich, Germany) for 10 min. Cells were permeabilised and blocked with bovine albumin (BSA; Sigma-Aldrich) supplemented with goat serum (Calbiochem, USA). Finally, the samples were dyed with phalloidin-fluorescein isothiocyanate (phalloidin-FITC). Microscopic analysis was performed using a LSM800 confocal microscope supplied with plan-apochromat 63 /1.4 oil DIC M27 lens and ZEN 2.1 software (Zeiss, Germany). The doxorubicin fluorescence emission was measured at 590 nm and the phalloidin-FITC staining the cytoskeleton at 488 nm.

2.9. Trypan blue exclusion test

To determine the viability of the treated cells, 1.3 10^6 cells were seeded in each well of a 24-well plate in complete RPMI 1640 medium w/o FA and cultured for 24 h. Then, growth medium was replaced with 500 ml of fresh medium supplemented with empty nanoparticles (7.2 mL/mL) or drug-loaded nanoparticles (7.2 mL/mL; DOX concentration - 1.4 mM). After 24 h of incubation, the cells were washed using Dulbecco's phosphate-buffered saline (D-PBS), trypsinized and centrifuged (200g, 5 min). The cell pellet was subsequently re-suspended in D-PBS and stained with trypan blue (0.2% (w/v); Sigma-Aldrich) for 10 min. In the next step, the number of viable (unstained) and non-viable cells (blue) was determined using an EVE automatic cell counter (NanoEnTek, South Korea). Viability was expressed as a percentage of unstained cells divided by the total number of cells.

2.10. In vitro cytotoxicity assay

Cytotoxicity analysis was performed using the CellTiter-96 AQueous-Non-Radioactive MTS assay (Promega, Germany) according to the manufacturer's protocol. Briefly, 24 h before the experiment, 3.0 10^3 cells were seeded in each well of a 96-well plate in complete RPMI 1640 medium w/o FA. After 24 h of incubation, the culture medium was replaced with 100 mL of fresh medium containing empty nanoparticles (7.2 mL/mL) or drugloaded nanoparticles (7.2 mL/mL; DOX

concentration - 1.4 mM) and further incubated for 24 h. Absorbance was measured at 490 nm using the microplate reader Apollo 11LB913 (Berthold, Germany). All treatments were performed in six replicates. To evaluate the percentage of metabolically active cells, control experiments were performed with the use of untreated cells (negative control) and this average absorbance was subtracted from the absorbance of wells containing the treated cells.

2.11. Flow cytometric analysis of cell apoptosis

The flow cytometry technique was used to detect apoptotic and necrotic cells in the treated samples. The experiment was performed according to the previously described procedure with some minor modifications [28]. Briefly, cells were seeded (5 10^5 cells/ well) in complete RPMI 1640 medium w/o FA in a 6-well plate and cultured for 24 h. Then, the medium was replaced with 2 mL of fresh medium supplemented with HEX/FA (7.2 mL/mL), HEX/DOX, and HEX/DOX/FA compounds (7.2 mL/mL; DOX concentration 1.4 mM). For folate receptor blocking, cells were seeded in RPMI 1640 medium supplemented with 10% FBS (Biological Industries) and 100 mg/mL antibiotics (Biological Industries) and subsequently treated with CUB/DOX/FA or HEX/DOX/FA. After 2 h, culture medium containing floating cells was collected in Falcon tube (15 mL). Next, the attached cells were trypsinized and then added to the same tube. Cells were then pelleted by centrifugation (200g, 5 min), re-suspended in 500 mL of binding buffer and finally incubated with 5 mL of Annexin V-FITC (BD Biosciences, USA) for 15 min at room temperature in the dark. Fluorescence intensities were analysed using flow cytometry (FACSCanto II, BD Biosciences) and BD FACSDiva software (BD Biosciences).

2.12. Statistical analysis

All experiments were performed at least three times. Numerical data are presented as mean ± SD. For statistical analysis Prism (version 5.04; GraphPad, Inc., USA) computer software was used. Data were analysed using One-way ANOVA or the Mann Whitney U test. Statistical significance was considered at $P < 0.05$.

3.Results and discussion

3.1. Sample characterization

All samples were analysed using SAXS technique, which offers qualitative information about the internal structure of each mesophase. The internal structure of LLC NPs, in terms of mesophase structure and lattice parameter, can be affected by various factors. High amounts of stabilizer, with respect to the amount of lipid, may change the lattice parameter. This also depends on the type of stabilizer, as in some cases, a more swollen Im3m phase may be formed. The commonly used Pluronic F108 was found to be the most effective stabilizer of GMO cubosomes, which retained their native double diamond cubic phase (Pn3m) structure. To determine the effect of using PF108-FA to form cubosomes and hexosomes, SAXS was applied. The SAXS spectra were converted into 1D scattering plots and the crystalline structure was determined by comparing the relative positions of the resulting peaks. To identify the phase type, the scattering vector (q) values of the peaks were correlated with Miller indices for known liquid crystalline phases. The lattice parameters (a) of the mesophases were calculated from the corresponding reciprocal spacing. Fig. 1A shows the SAXS spectra obtained for the empty and drug-loaded cubosome formulations. The 1D diffraction patterns for samples showed reflections in the ratios of √2, √3, √4, √6, √8, √9, which are characteristic for the cubic-Pn3m phase. All six Bragg reflections were observed for the CUB formulations, in the absence or presence of DOX or PF108-FA. The X-ray patterns were best fitted to the cubic Pn3m phase with lattice parameter close to 10.2 nm at 25 C either for the non-doped or DOX-doped mesophase. Lattice parameters were similar for all samples, thus it was concluded that such modifications of mesophase LCP do not affect the structure of the samples. Moreover, it was determined that for the used concentration, the penetration of lipid dispersion by PF 108-FA does not affect the structure of all samples.

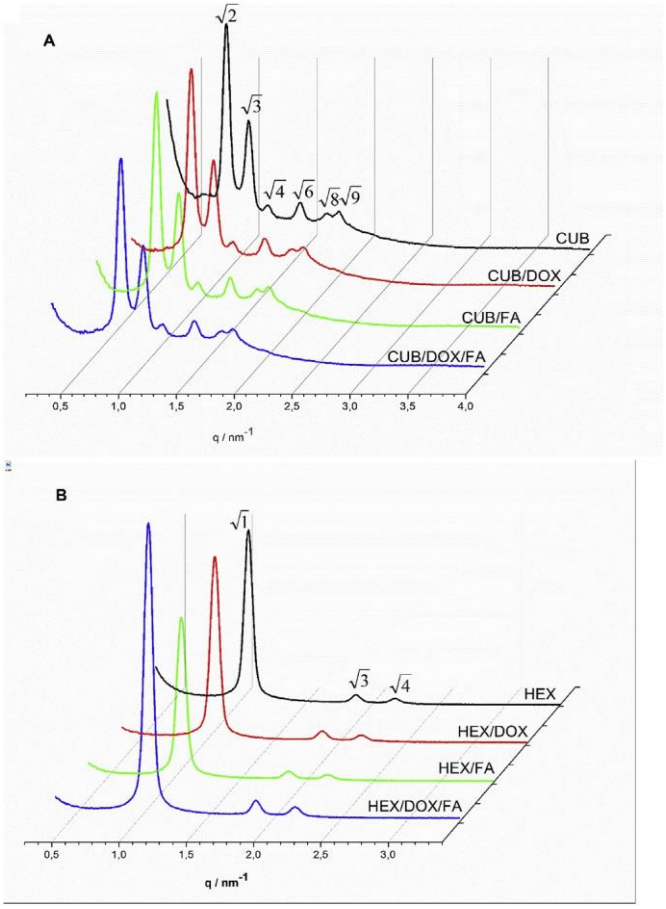

Fig. 1. 1D diffraction patterns of cubosomes (A) and hexosomes (B).

Fig. 1B shows the q (nm^{1}) vs. intensity plots for the GMO/TD dispersions obtained from the SAXS 2D diffraction patterns. As predicted using the critical packing parameter (CPP) approach, hydrophobic tetradecane added to monoolein induced the formation of a more negatively curved hexagonal structure. The SAXS technique was applied to identify the internal structure of hexosomes. The Bragg peaks were indexed allowing for the confirmation of the structures. As expected, three Bragg reflections in the ratio 1:√3:√4, which corresponds to the H2 phase, were observed. The lattice parameter (a) that corresponds to the distance between two cylinders is described by the equation: a ¼ 4dðh^2 þ k^2 þ hkÞ$^{1=2}$, where q_{hk} are the position of each peak defined by hk Miller indices. The X-ray patterns were best fitted to the hexagonal phase with lattice parameter 6.6 nm at 25 C either for the non-doped or DOX-doped mesophase.

Based on the SAXS analysis, we concluded that DOX-loaded cubosomes and hexsosomes, stabilized with folate-functionalized PF108, retained the structure of unmodified cubosomes or hexosomes, respectively. SAXS results also confirmed that the effect of folic acid or DOX on the structure of the cubic phase is modest.

The composition of the investigated samples, the lattice parameters derived from SAXS data analysis and the identified liquid crystalline phases are presented in Table 1. The dynamic light scattering measurements provide information on the hydrodynamic size of cubic and hexagonal dispersions, while the polydispersity index (PDI) value indicates stability of cubic and hexagonal NPs against aggregation. The hydrodynamic size of CUB/ DOX/FA dispersion is 152 ± 11 nm with a PDI value close to 0.2. The average particle diameter of HEX/DOX/FA is 178 ± 28 nm with PDI 0.22. The obtained PDI values of NPs indicate homogeneity of the formulations. Both CUB and HEX nanocarriers exhibit high drugloading efficiency with values of 90%.

3.2. Electrochemical characterization of doxorubicin incorporated into lipid mesophases - in vitro release study

The internal structure of lipid mesophases (cubosomes and hexosomes) is able to host cargos of different hydrophobicity and hydrophilicity. However, the open structure of cubosomes with water channels exposed to the aqueous solution assures fast drug release (which can diffuse out of the phase) while closed water channels in hexosomes slow down drug diffusion [10,24].

The drug release profile from DOX-loaded folate-conjugated dispersed systems, was determined using electrochemical methods. To obtain the release profile from dispersed systems, nanoparticles loaded with DOX, or free DOX (at the same quantity as DOX in nanoparticles), were placed in the dialysis membrane (MWCO 12e14 kDa) and submerged in 50 ml of deoxygenated MES buffer pH 5.6. A dialysis membrane was used also to prevent adsorption of lipids and polymers on the working electrode.

Table 1
Properties of the nanoparticles formulations.

Nanoparticle and dopant used	Symmetry	Unit Cell 25 C [nm]	Size [nm]	PDI index	EE [%]
CUB NPs	Pn3m (V2)	10.15	158 ± 3	0.16 ± 0.04	e
CUB/DOX NPs	Pn3m (V2)	10.32	154 ± 9	0.12 ± 0.03	92 ± 3
CUB/FA NPs	Pn3m (V2)	10.15	156 ± 11	0.14 ± 0.03	e
CUB/DOX/FA NPs	Pn3m (V2)	10.24	152 ± 11	0.20 ± 0.05	93 ± 4
HEX NPs	p6m (H2)	6.62	179 ± 14	0.22 ± 0.02	e
HEX/DOX NPs	p6m (H2)	6.61	180 ± 12	0.22 ± 0.02	85 ± 6
HEX/FA NPs	p6m (H2)	6.62	177 ± 20	0.26 ± 0.02	e
HEX/DOX/FA NPs	p6m (H2)	6.62	178 ± 28	0.22 ± 0.02	82 ± 3

DOX is a redox-active drug molecule with one quinone (Q) and one hydroquinone (QH2) group and the redox properties of DOX were described in more detail in our previous article [24]. DOX underwent reduction at ca. 0.56 V, which corresponds to the reduction of the 5,12-diquinone groups of DOX while irreversible oxidation of the hydroquinone center occurs at þ0.74 V. Reduction is related to the Q/QH_2 redox pairs: Q þ 2e þ 2Hþ 4 QH_2 that undergoes a $2e^{e}/2H$þ conversion. Due to better reversibility and reproducibility, the reduction peak was selected to determine the release profile (Fig. 2A). To detect the amount of drug released, SW voltammetry was applied. SWV was selected since it combines excellent sensitivity and the rejection of background currents together with the high speed of measurements that allows for experiments to be performed repetitively. This technique enabled collecting scans in short intervals of time and allowed monitoring the drug releasing profile from the cubosome/hexosome dispersions with high accuracy. Fig. 2B shows the representative SW voltammograms recorded after 200 min of drug release from DOXcontaining dispersions of hexosomes and cubosomes. After 200 min, it was observed that more DOX was released from the cubosome dispersion, whereas in the hexosome NPs, the drug remained in the lipid matrix.

The DOX release profile is presented as a function of time in Fig. 2C. Compared to free DOX, the release of DOX from folateconjugated nanoparticles was prolonged, but also depended on the structure of the mesophase. Less DOX was released from HEX/ DOX/FA, when compared to CUB/DOX/FA (and free drug). A very slow-release profile, without an initial burst release of the drug, was observed for HEX/DOX/FA dispersion. In case of CUB/DOX/FA, an initial burst release was observed. This behavior is connected with the properties of the drug, as at pH 5.6, DOX is expected to be located in the water channel, where diffusion is faster than in the lipid domain. Similar behavior was observed for non-functionalized with FA nanoparticles [data not shown]. Comparing the release properties for both mesophases, we can conclude that the release rate is affected by the phase structure of the mesophase and that the ability of the hexagonal phase to slow down the rate of DOX release may be potentially used for sustained drug delivery. Application of CUB/DOX/FA results in the increased drug release rate, in comparison to the HEX/DOX/FA. This indicates that the structure of the mesophase is a key factor that controls the release of DOX embedded in the mesophase.

To quantify the release and to determine the release kinetics the current values were normalized with respect to the current measured for free DOX (we chose the current for the free DOX as I_{max} under the same conditions as the LLC dispersions) [Fig. 3A]. In the case of lipid mesophases diffusion of soluble drugs occurs within the aqueous channels, thus release from nanoparticles was expected to be purely Fickian. The drug release data were fitted into Higuchi's equation: $M_t=M_\infty$ ¼ kpt , where M_t/M_∞ is a fraction of drug released at time t, and k is the release rate constant. In this model, the cumulative drug release is proportional to the square root of time [Fig. 3B].

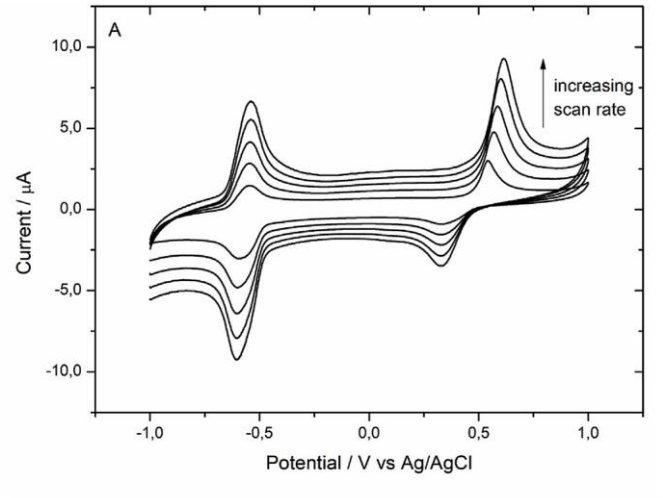

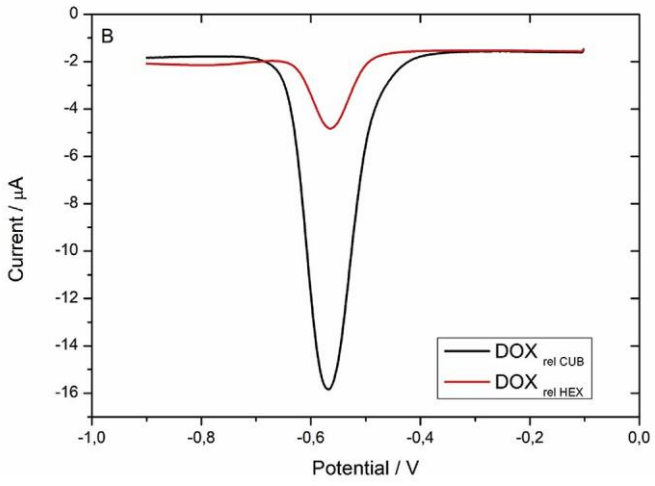

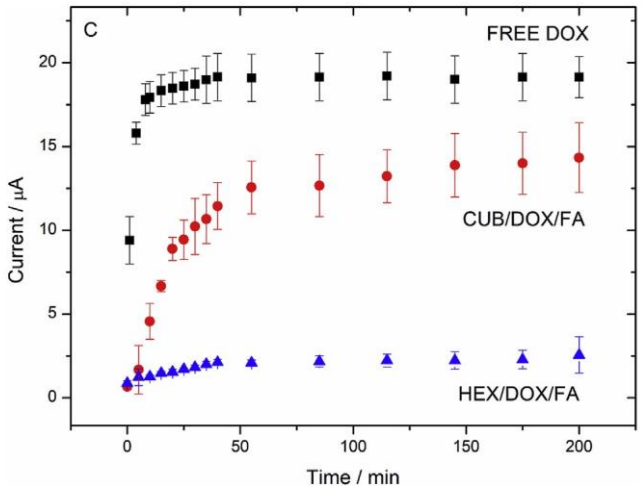

Fig. 2. (A) Cyclic voltammogram for DOX in 0.1 M MES buffer. Scan rate: from 20 mV s^{1} to 100 mVs^{1}, pH 5.6. (B) DP voltammogram recorded on GCE after 200 min of DOX release form DOX-containing dispersions of hexosomes (HEX) and cubosomes (CUB). Amplitude: DE ¼ 50 mV, pulse time: tp ¼ 50 ms. (C) Current vs. time plot of DOX release from DOX loaded CUB/FA, HEX/FA and free DOX.

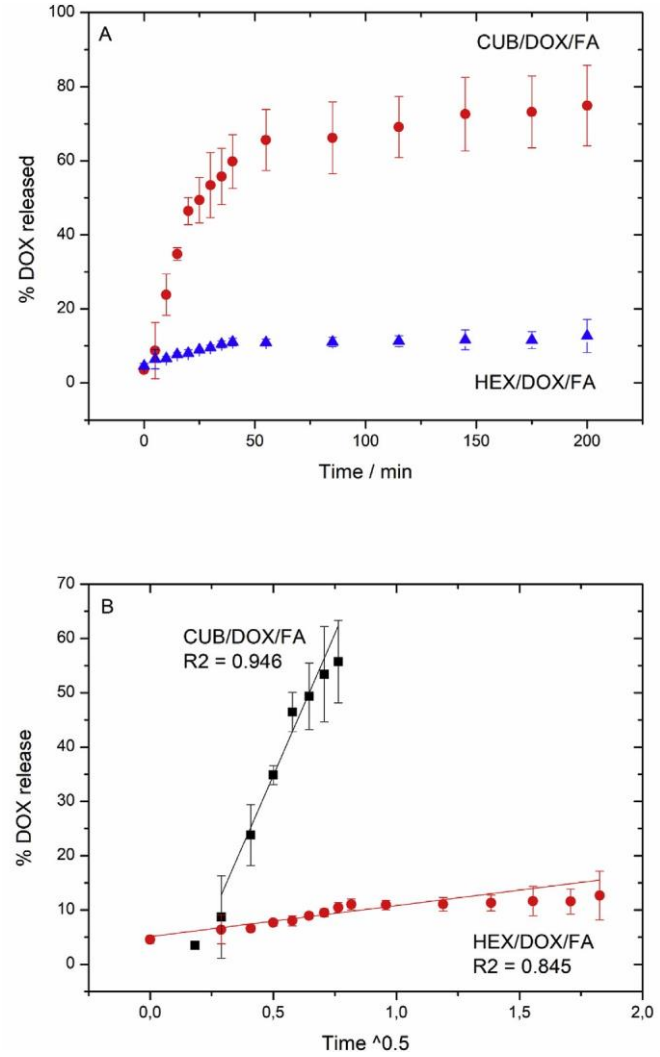

Fig. 3. (A) The current normalized release profile of DOX from the dispersed mesophases. (B) Higuchi release model.

The highest value of the correlation coefficient for Higuchi model was observed for CUB/DOX/FA dispersion (R^2 ¼ 0.946). The high correlation coefficient observed for the CUB/ DOX/FA formulation suggests that DOX transport in cubosomes is controlled by diffusion. In case of HEX/DOX/FA the R^2 was lower (R^2 ¼ 0.845), indicating that the hexagonal structure may affect the drug transport properties.

3.3. Fluorescence analysis of DOX intake by cancer cells

To investigate the efficacy of folate-targeted lipid mesophases, three human-derived cell lines: KB, HeLa and T98G were used. The yield of folate receptor was evaluated using the Western blot method. We confirmed that both KB and HeLa cells are FR-positive (express a high level of folate receptor protein), as expected [29e32]. In contrast, the expression of folate receptor in T98G cells was negligible (Fig. 4). Therefore, the T98G cell line was used as a negative control.

To determine the DOX delivery capability of the studied folatetargeted lipid mesophases, fluorescence analysis of the treated cancer cells was performed. DOX presents natural fluorescence, therefore it was expected that the measured fluorescence intensity would be positively correlated with intake of DOX-loaded nanocarriers by the tested cells.

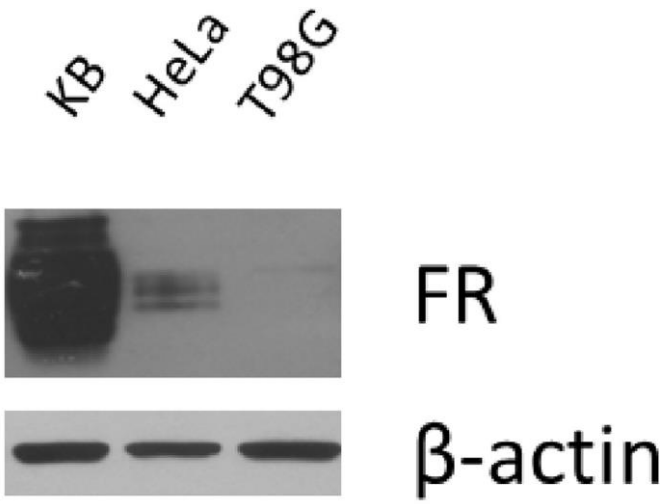

Fig. 4. Western blot analysis of folate receptor (FR) protein expression in KB, HeLa and T98G cells. For each lane, 20 mg of crude protein extract was loaded. b-actin served as a loading control.

The DOX fluorescence properties were quantified in crude protein extracts obtained from cells treated with DOX-loaded nanocarriers (as described in the Experimental section). The highest DOX accumulation was observed for KB and HeLa cells treated with folate-functionalized DOX-loaded cubosomes (Fig. 5). In case of folate-modified hexosomes, DOX intake was lower in comparison to cubosomes. This may be explained by the difference between hexosomes and cubosomes in the drug release properties. Since water channels are closed in the hexagonal structure, the release of DOX is sustained leading to lower accessibility of the drug. In contrast, T98G cancer cells treated with CUB/ DOX/FA or HEX/DOX/FA exhibited similar levels of DOX intake when compared with non-FA-targeted structures.

The accumulation of doxorubicin in KB, HeLa and T98G cells exposed to DOX-loaded nanoparticles was further examined using confocal microscopy (Fig. 6). The cells were cultured in complete RPMI 1640 medium w/o FA or in complete normal RPMI 1640 medium and then treated with CUB/DOX, HEX/DOX, CUB/DOX/FA or HEX/DOX/FA, respectively. A set of treated cells incubated in normal RPMI 1640 medium served as an additional internal control. Complete RPMI 1640 medium contains a higher concentration (2.26 mM) of FA, as opposed to the very low concentration of FA (3 nM) in complete RPMI 1640 medium w/o FA. Therefore, it was expected that FA present in the normal medium would block the cell's folic acid receptors and significantly reduce the binding ability of the tested FA-tagged carriers [32]. Overall, the intracellular DOX intake observed in the studied cells corresponded well to the DOX yield measured in the total protein lysates. The highest intracellular concentration of doxorubicin was observed in KB and HeLa cells treated with the DOX-loaded CUB/FA carrier. Though HEX/FAtreated cells also presented some increase in intracellular DOX accumulation, it was still lower than the one observed for the DOXloaded cubic phase (Fig. 6). Such a pattern stays in accordance with previously published studies describing drug delivery capabilities of the hexagonal phase. It has been reported that cubosomes present a higher DOX-delivery ability than hexosomes [24]. Interestingly, pre-incubation of KB and HeLa cells with normal medium resulted in a significant reduction of DOX delivery. The observed decrease in intracellular DOX accumulation of both DOX-loaded cubosomes and hexosomes was likely a consequence of folate receptors being blocked by free FA present in normal medium. In contrast, the intracellular DOX accumulation in all the tested T98G cells was similar (as expected) due to T98G cells lacking FR.

3.4. In vitro cytotoxicity and viability assessment

In order to determine the anticancer activity of DOX-loaded CUB/HEX and CUB/HEX/FA formulations, in vitro cell cytotoxicity was evaluated using MTS assay. The obtained data indicate that after 24 h of incubation (Fig. 7AeC), empty folate-targeted cubosomes and hexosomes were non-toxic to KB, HeLa and T98G cells. Whereas, as shown in Fig. 7DeE, after 24-h incubation with nontargeted CUB/DOX, 35% and 76% of KB and HeLa cells, respectively, were still metabolically active. Encapsulation of DOX in the folate-modified cubic phase resulted in reduction of the survival rate of KB and HeLa cells, in comparison to CUB/DOX-treated cells (16% and 57%, respectively). While exposition of KB cells to folatetargeted hexosomes did not show significant reduction in cell viability, compared to HEX/DOX, the DOX/HEX/FA effect was observed in HeLa cells. FA-mediated cytotoxicity in T98G cells was similar in both drug-loaded cubic and hexagonal phases when compared with non-targeted carriers [Fig. 7F].

Moreover, the viability of the tested cancer cells treated with various DOX-loaded nanocarriers was examined using the trypan blue exclusion assay (Fig. 8DeF). In accordance to the MTS data, it was observed that the survival rate of both KB and HeLa cells exposed to CUB/DOX/FA was lower than in case of cells treated with CUB/DOX nanoparticles (Fig. 8DeE). Similarly, the viability of HeLa cells exposed to DOX encapsulated in HEX/FA was reduced more significantly than the viability of cells treated with the non-FAlabelled hexagonal phase (Fig. 8E). In case of KB cells, the effect of HEX/DOX/FA on the cell viability was less evident (Fig. 8D). Some minor inconstancies between the cytotoxicity and viability data were likely due to limitations of the applied methodologies.

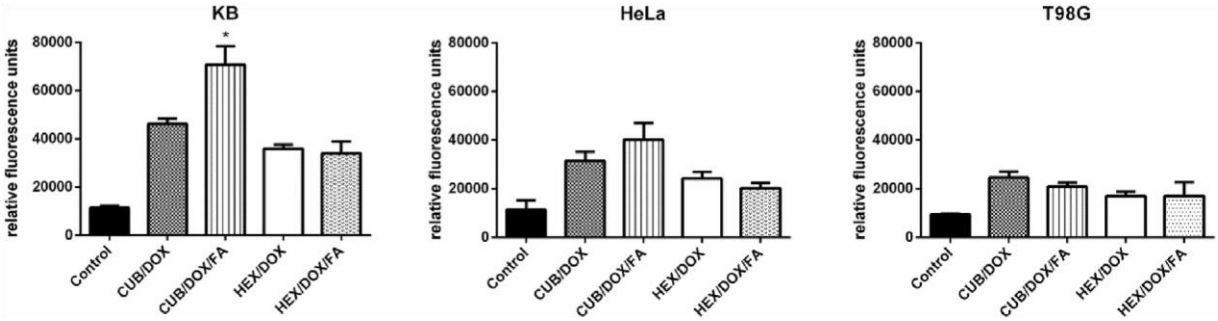

Fig. 5. Intracellular intake of doxorubicin by KB, HeLa and T98G cells treated for 2 h with DOX-loaded nanoparticles (CUB/DOX or HEX/DOX) or DOX-loaded nanoparticles conjugated with folic acid (CUB/DOX/FA or HEX/DOX/FA) determined by fluorescence intensity measurements in crude protein extracts. Non-treated cells were used as a control. CUB, cubosome; FA, folic acid; HEX, hexosome.

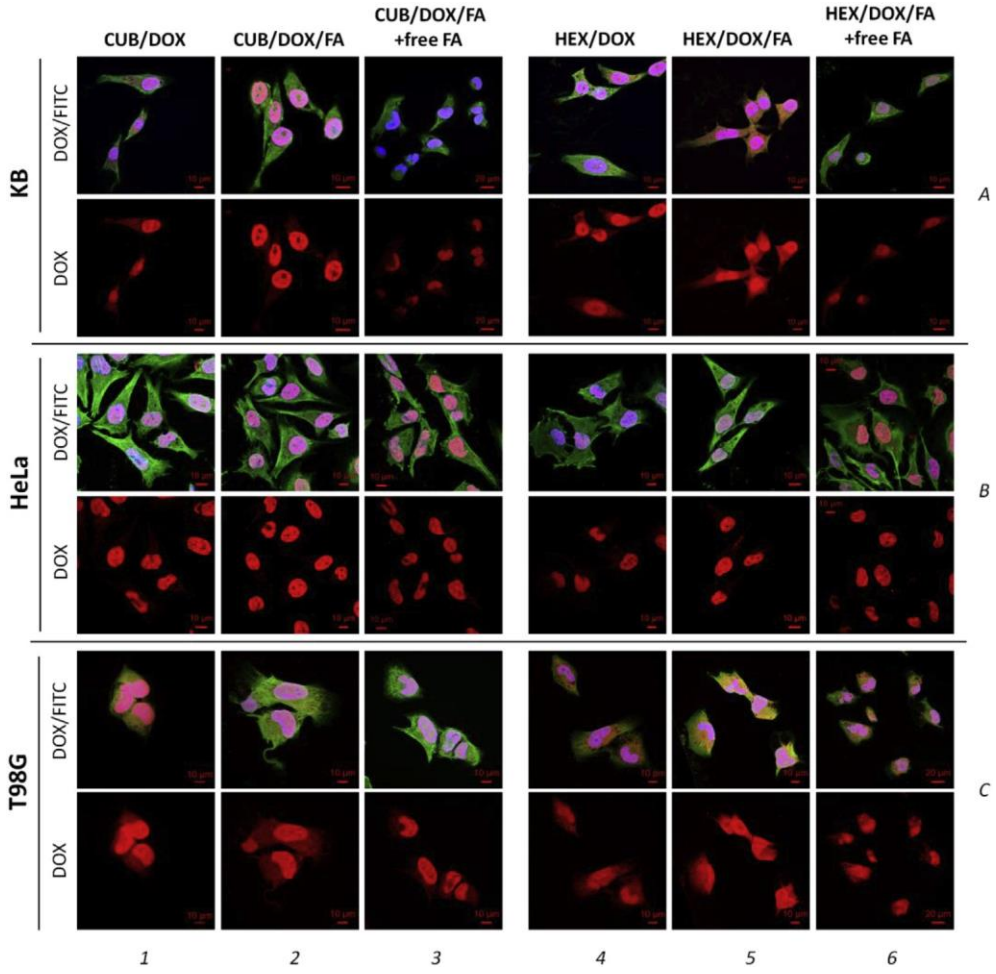

Fig. 6. Confocal analysis of FA-mediated delivery of drug encapsulated in cubic or hexagonal phases into KB, HeLa and T98G cells treated with doxorubicin-loaded nanoparticles (CUB/DOX or HEX/DOX) or FA-conjugated vectors (CUB/DOX/FA or HEX/DOX/FA) for 2 h. Cells incubated in the presence of a high concentration of FA (þfree FA) served as controls. Representative fluorescence images show subcellular DOX (red) distribution and actin stress fibers (green) organization in the tested cells. Actin microfilaments were stained with phalloidin-FITC (fluorescein isothiocyanate). CUB, cubosome; FA, folic acid; HEX, hexosome. (For interpretation of the references to colour in this figure legend, the reader is referred to the Web version of this article.)

The MTS assay specifically measures mitochondrial activity that occurs only in viable, proliferating cells, while the viability assay is designed to only distinguish between necrotic (dye permeable) and viable cells (dye non-permeable). As expected, the viability of FRnegative T98G cells was not affected by FA-functionalized particles. Additionally, the performed control experiments confirmed that folic acid-functionalized empty nanoparticles are not harmful for the tested cells (Fig. 8AeC).

DOX intake and viability assays demonstrated a less evident response of FR-positive cells to FA-tagged hexosomes than to CUB/ DOX/FA. This could be explained by the prolonged drug release capability of the hexagonal phase conjugated with folic acid. To confirm this phenomenon, Annexin V-FITC-based

staining assay, followed by flow cytometric analysis, was performed. Cells were treated with HEX/DOX or HEX/DOX/FA carriers and apoptosis/necrosis rates were determined (Fig. 9). After a 2-h incubation, treatment with DOX-loaded hexosomes showed increase in apoptosis/necrosis of KB and HeLa cells. Nevertheless, the most significant induction of death-leading processes was observed after treatment of both HeLa and KB cells with HEX/DOX/FA. Importantly, saturation of the folate receptor with an excess concentration of FA effectively withdrew this effect in both KB and HeLa cells (Fig. 9). Consequently, the FA-conjugated DOX-loaded hexagonal phase presented no significant effect on apoptosis/necrosis of T98G cells due to negligible expression of the folate receptor.

4. Conclusion

Folate receptor is overexpressed in many tumor types, and thereby, is considered as a potential molecule for development of targeted cancer therapies. It can be exploited to deliver therapeutic compounds directly to cancerous tissues. Here, we evaluated the efficacy of folate-targeted lipid mesophases in three humanderived cell lines exhibiting different expressional levels of folate receptor protein. Phase identity and structural parameters of folatetargeted mesophases were verified through small-angle X-ray scattering, while DOX release profiles of nanoparticles were monitored electrochemically. We found that the structure of the mesophase is a key factor that controls the release of DOX embedded in the mesophase. Controlled/sustained drug releasing can be realized by choosing a proper mesophase system. The FRfunctionalized hexosomes showed a slow DOX discharge profile without an initial burst release of the drug observed for the cubosomes. The DOX release from FA-nanoparticles was dependent on the square root of time and the Higuchi model was used to describe the kinetics.

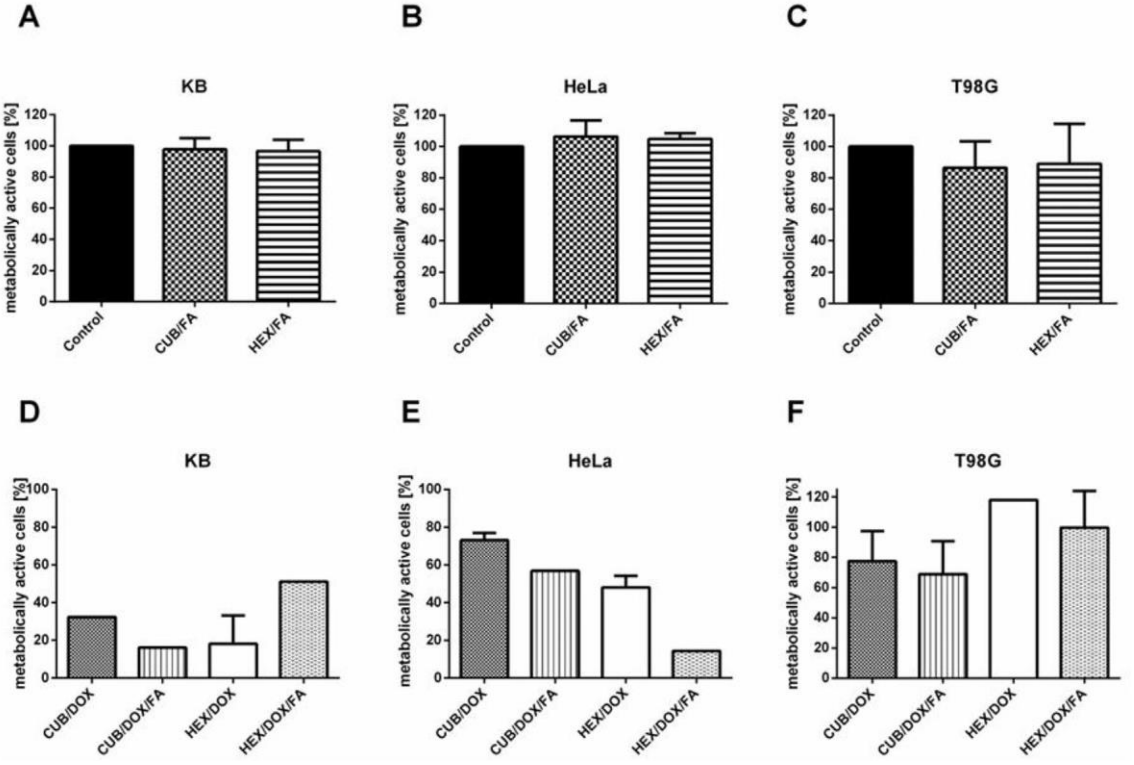

Fig. 7. Metabolic activity of KB, HeLa and T98G cells treated with empty nanoparticles conjugated with folic acid (CUB/FA or HEX/FA), DOX-loaded nanoparticles (CUB/DOX or HEX/ DOX) or DOX-loaded nanoparticles conjugated with folic acid (CUB/DOX/FA or HEX/DOX/FA) for 24 h determined by MTS assay. Non-treated cells and treated with CUB/DOX or HEX/ DOX were used as controls. CUB, cubosome; FA, folic acid; HEX, hexosome.

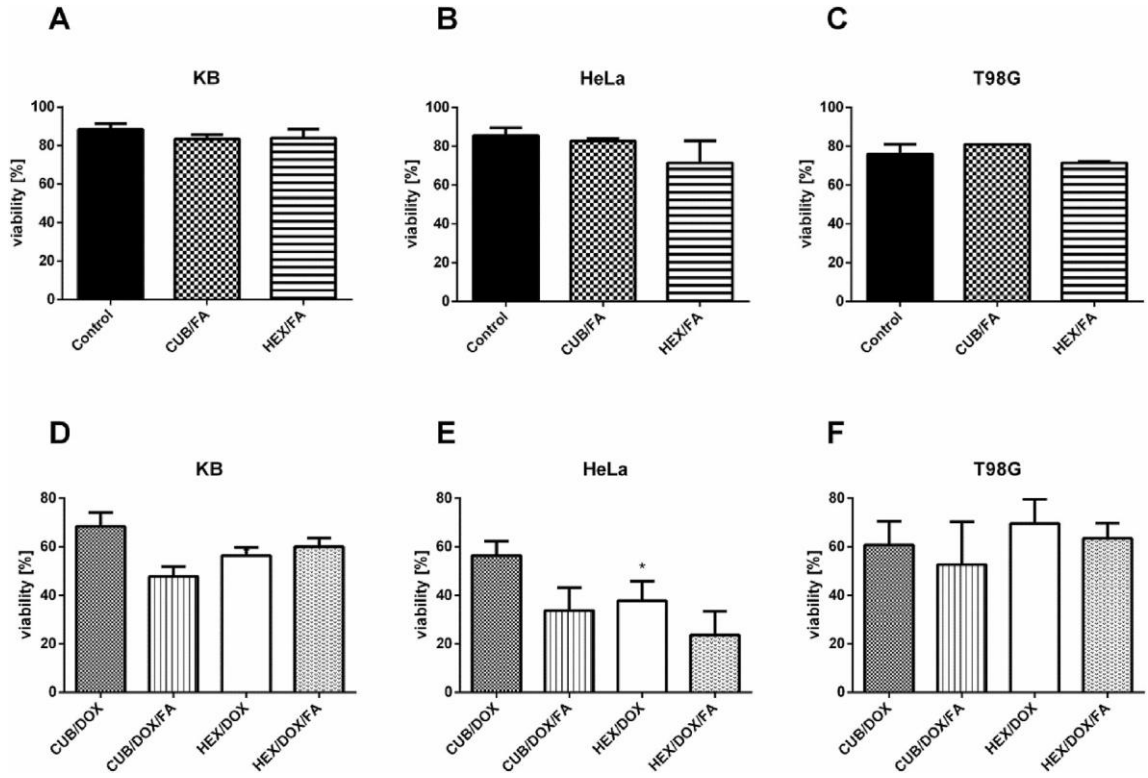

Fig. 8. Cell viability of KB, HeLa and T98G treated cells determined by the trypan blue exclusion assay. Cells were treated with empty nanoparticles conjugated with folic acid (CUB/ FA or HEX/FA), DOX-loaded nanoparticles (CUB/DOX or HEX/DOX) or DOX-loaded nanoparticles conjugated with folic acid (CUB/DOX/FA or HEX/DOX/FA) for 24 h. Non-treated and CUB/DOX- or HEX/DOX-treated cells were used as controls. CUB, cubosome; FA, folic acid; HEX, hexosome.

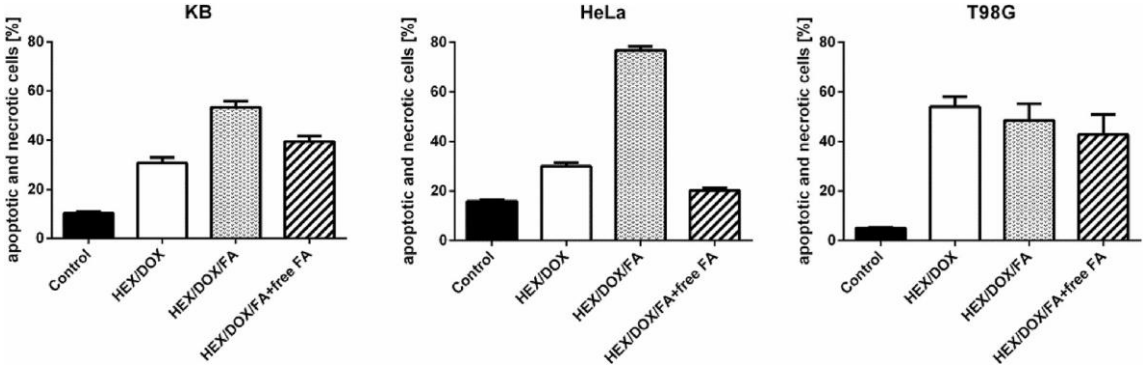

Fig. 9. The percentage of apoptotic and necrotic KB, HeLa and T98G cells after treatment for 2 h with DOX-loaded hexosomes (HEX/DOX), DOX-loaded hexosomes conjugated with folic acid (HEX/DOX/FA) or HEX/DOX/FA blocked with free FA, determined by flow cytometry. Non-treated cells were used as a control. HEX, hexosome; FA, folic acid

Fluorescence-based analyses revealed that the treatment of FR-positive HeLa and KB cells with folate-modified hexosomes results in lower intracellular DOX intake when compared to folate-targeted DOX-loaded cubosomes. These data stay in accordance with the reported characteristics of DOX release from cubosomal and hexosomal mesophases, where the DOX release from hexosomes was sustained, leading to lower accessibility of the drug. The viability assays showed that the administration of CUB/FA-encapsulated DOX to HeLa and KB cells rapidly decreased their survival rate and improved drug-mediated antitumor activity. These results show that bioconjugation of FA to cubosomes and hexosomes has a promising potential in effective delivery of chemotherapeutic agents to folate-overexpressing tumors.

Acknowledgements

Mirosław Salamonczyk is acknowledged for help with SAXS experiments. This work was financially supported by the National Science Centre, Poland (Project No. 2016/23/B/ST4/03295). EN acknowledges support from the National Science Centre, Poland (Project No. 2017/25/B/ST4/02817).

Appendix A. Supplementary data

Supplementary data to this article can be found online at https://doi.org/10.1016/j.electacta.2018.12.164.

References

[1] V. Luzzati, F. Husson, The structure of the liquid-crystalline phases of lipidwater systems, J. Cell Biol. 12 (1962) 207e219. https://doi.org/10.1083/jcb. 12.2.207.

[2] A. Angelova, B. Angelov, R. Mutafchieva, S. Lesieur, P. Couvreur, Self-Assembled multicompartment liquid crystalline lipid carriers for protein, peptide, and nucleic acid drug delivery, Acc. Chem. Res. 44 (2011) 147e156. https:// doi.org/10.1021/ar100120v.

[3] W.-K. Fong, R. Negrini, J.J. Vallooran, R. Mezzenga, B.J. Boyd, Responsive selfassembled nanostructured lipid systems for drug delivery and diagnostics, J. Colloid Interface Sci. 484 (2016) 320e339. https://doi.org/10.1016/j.jcis. 2016.08.077.

[4] S.J. Fraser, X. Mulet, A. Hawley, F. Separovic, A. Polyzos, Controlling nanostructure and lattice parameter of the inverse bicontinuous cubic phases in functionalised phytantriol dispersions, J. Colloid Interface Sci. 408 (2013) 117e124. https://doi.org/10.1016/j.jcis.2013.07.002.

[5] S. Phan, W.-K. Fong, N. Kirby, T. Hanley, B.J. Boyd, Evaluating the link between self-assembled mesophase structure and drug release, Int. J. Pharmacol. 421 (2011) 176e182. https://doi.org/10.1016/j.ijpharm.2011.09.022.

[6] R. Negrini, R. Mezzenga, PH-responsive lyotropic liquid crystals for controlled drug delivery, Langmuir 27 (2011) 5296e5303. https://doi.org/10.1021/ la200591u.

[7] B.J. Boyd, W.-K. Fong, Stimuli-responsive lipid-based self-assembled systems, Self-Assembled Supramol. Architect.: Lyotrop. Liquid Cryst. (2012) 257e288. https://doi.org/10.1002/9781118336632.ch9.

[8] R. Negrini, A. Sanchez-Ferrer, R. Mezzenga, In fluence of electrostatic interactions on the release of charged molecules from lipid cubic phases, Langmuir 30 (2014) 4280e4288. https://doi.org/10.1021/la5008439.

[9] J. Clogston, M. Caffrey, Controlling release from the lipidic cubic phase. Amino acids, peptides, proteins and nucleic acids, J. Contr. Release 107 (2005) 97e111. https://doi.org/10.1016/j.jconrel.2005.05.015.

[10] S. Phan, W.-K. Fong, N. Kirby, T. Hanley, B.J. Boyd, Evaluating the link between self-assembled mesophase structure and drug release, Int. J. Pharmacol. 421 (2011) 176e182. https://doi.org/10.1016/j.ijpharm.2011.09.022.

[11] W.-K. Fong, T. Hanley, B.J. Boyd, Stimuli responsive liquid crystals provide 'ondemand' drug delivery in vitro and in vivo, J. Contr. Release 135 (2009) 218e226. https://doi.org/10.1016/j.jconrel.2009.01.009.

[12] J.N. Israelachvili, D.J. Mitchell, B.W. Ninham, Theory of self-assembly of lipid bilayers and vesicles, BBA e Biomembranes 470 (1977) 185e201. https://doi. org/10.1016/0005-2736(77)90099-2.

[13] V. Cherezov, J. Clogston, M.Z. Papiz, M. Caffrey, Room to move: Crystallizing membrane proteins in swollen lipidic mesophases, J. Mol. Biol. 357 (2006) 1605e1618. https://doi.org/10.1016/j.jmb.2006.01.049.

[14] B. Angelov, A. Angelova, R. Mutafchieva, S. Lesieur, U. Vainio, V.M. Garamus, G.V. Jensen, J.S. Pedersen, SAXS investigation of a cubic to a sponge (L3) phase transition in self-assembled lipid nanocarriers, Phys. Chem. Chem. Phys. 13 (2011) 3073e3081. https://doi.org/10.1039/c0cp01029d.

[15] N. Alcaraz, Q. Liu, E. Hanssen, A. Johnston, B.J. Boyd, Clickable cubosomes for antibody-free drug targeting and imaging applications, Bioconjug. Chem. 29 (2018) 149e157. https://doi.org/10.1021/acs.bioconjchem.7b00659.

[16] J. Zhai, R.B. Luwor, N. Ahmed, R. Escalona, F.H. Tan, C. Fong, J. Ratcliffe, J.A. Scoble, C.J. Drummond, N. Tran, Paclitaxel-loaded self-assembled lipid nanoparticles as targeted drug delivery systems for the treatment of aggressive ovarian cancer, ACS Appl. Mater. Interfaces 10 (2018) 25174e25185. https://doi.org/10.1021/acsami.8b08125.

[17] S. Aleandri, D. Bandera, R. Mezzenga, E.M. Landau, Biotinylated cubosomes: a versatile tool for active targeting and codelivery of paclitaxel and a fluorescein-based lipid dye, Langmuir 31 (2015) 12770e12776. https://doi. org/10.1021/acs.langmuir.5b03469.

[18] C. Caltagirone, A.M. Falchi, S. Lampis, V. Lippolis, V. Meli, M. Monduzzi, L. Prodi, J. Schmidt, M. Sgarzi, Y. Talmon, R. Bizzarri, S. Murgia, Cancer-celltargeted theranostic cubosomes, Langmuir 30 (2014) 6228e6236. https://doi. org/10.1021/la501332u.

[19] Y. Tian, J.C. Li, J.X. Zhu, N. Zhu, H.M. Zhang, L. Liang, L. Sun, Folic acid-targeted etoposide cubosomes for theranostic application of cancer cell imaging and therapy, Med. Sci. Monit. 23 (2017) 2426e2435. https://doi.org/10.12659/ MSM.904683.

[20] V. Meli, C. Caltagirone, C. Sinico, F. Lai, A.M. Falchi, M. Monduzzi, M. ObiolsRabasa, G. Picci, A. Rosa, J. Schmidt, Y. Talmon, S. Murgia, Theranostic hexosomes for cancer treatments: an in vitro study, New J. Chem. 41 (2017) 1558e1565. https://doi.org/10.1039/c6nj03232j.

[21] E. Nazaruk, M. Szle˛zak, E. Gorecka, R. Bilewicz, Y.M. Osornio, P. Uebelhart, E.M. Landau, Design and assembly of pH-sensitive lipidic cubic phase matrices for drug release, Langmuir 30 (2014) 1383e1390. https://doi.org/10.1021/ la403694e.

[22] E. Nazaruk, P. Miszta, S. Filipek, E. Gorecka, E.M. Landau, R. Bilewicz, Lyotropic cubic phases for drug delivery: diffusion and sustained release from the mesophase evaluated by electrochemical methods, Langmuir 31 (2015) 12753e12761. https://doi.org/10.1021/acs.langmuir.5b03247.

[23] E. Nazaruk, A. Majkowska-Pilip, R. Bilewicz, Lipidic cubic-phase nanoparticlescubosomes for efficient drug delivery to cancer cells, ChemPlusChem 82 (2017) 570e575. https://doi.org/10.1002/cplu.201600534.

[24] E. Nazaruk, A. Majkowska-Pilip, M. Godlewska, M. Salamonczyk, D. Gawel, Electrochemical and biological characterization of lyotropic liquid crystalline phases - retardation of drug release from hexagonal mesophases, J. Electroanal. Chem. 813 (2018) 208e215. https://doi.org/10.1016/j.jelechem.2018.01.029.

[25] M. Colombo, L. Fiandra, G. Alessio, S. Mazzucchelli, M. Nebuloni, C. De Palma, K. Kantner, B. Pelaz, R. Rotem, F. Corsi, W.J. Parak, D. Prosperi, Tumour homing and therapeutic effect of colloidal nanoparticles depend on the number of attached antibodies, Nat. Commun. 7 (2016) 13818. https://doi.org/10.1038/ ncomms13818.

[26] C.V. Kulkarni, W. Wachter, G. Iglesias-Salto, S. Engelskirchen, S. Ahualli, Monoolein: a magic lipid? Phys. Chem. Chem. Phys. 13 (2011) 3004e3021. https://doi.org/10.1039/c0cp01539c.

[27] M. Godlewska, W. Krasuska, B. Czarnocka, Biochemical properties of thyroid peroxidase (TPO) expressed in human breast and mammary-derived cell lines, PLoS One 13 (2018), e0193624. https://doi.org/10.1371/journal.pone. 0193624.

[28] A. Majkowska-Pilip, M. Rius, F. Bruchertseifer, C. Apostolidis, M. Weis, M. Bonelli, M. Laurenza, L. Krolicki, A. Morgenstern, In vitro evaluation of ^{225}Ac-DOTA-substanceP for targeted alpha therapy of glioblastma multiforme, Chem. Biol. Drug Des. 92 (2018) 1344e1356. https://doi.org/10.1111/cbdd. 13199.

[29] N. Parker, M.J. Turk, E. Westrick, J.D. Lewis, P.S. Low, C.P. Leamon, Folate receptor expression in carcinomas and normal tissues determined by a quantitative radioligand binding assay, Anal. Biochem. 338 (2005) 284e293. https://doi.org/10.1016/j.ab.2004.12.026.

[30] H. Chen, R. Ahn, J. Van den Bossche, D.H. Thompson, T.V. O'Halloran, Folatemediated intracellular drug delivery increases the anticancer efficacy of nanoparticulate formulation of arsenic trioxide, Mol. Canc. Therapeut. 8 (2009) 1955e1963. https://doi.org/10.1158/1535-7163.MCT-09-0045.

[31] S. Gorle, M. Ariatti, M. Singh, Novel serum-tolerant lipoplexes target the folate receptor efficiently, Eur. J. Pharm. Sci. 59 (2014) 83e93. https://doi.org/10. 1016/j.ejps.2014.04.012.

[32] Y. Yang, F. An, Z. Liu, X. Zhang, M. Zhou, W. Li, X. Hao, C.S. Lee, X. Zhang, Ultrabright and ultrastable near-infrared dye nanoparticles for in vitro and in vivo bioimaging, Biomaterials 33 (2012) 7803e7809. https://doi.org/10.1016/j.biomaterials.2012.07.006.